Journal of Geophysical Research: Oceans

RESEARCH ARTICLE
10.1029/2018JC013819

Sediment Resuspension Due to Near-Bed Turbulent Effects: A Deep Sea Case Study on the Northwest Continental Slope of Western Australia

Sarik Salim[1], **Charitha Pattiaratchi**[1], **Rafael O. Tinoco**[2], **and Ravindra Jayaratne**[3]

[1]Oceans Graduate School and UWA Oceans Institute, University of Western Australia, Perth, Western Australia, Australia, [2]Department of Civil and Environmental Engineering, University of Illinois at Urbana-Champaign, Urbana, IL, USA, [3]School of Architecture, Computing and Engineering, University of East London, London, UK

Key Points:
- In deep ocean systems, sediment resuspension occurs even when mean velocities are below the time-averaged critical velocity
- On the continental slope, sediment flux is largely controlled by ejection and sweep turbulent events
- Wavelet transforms indicated turbulent bursting associated with intense sediment resuspension

Correspondence to:
S. Salim,
sarik.salim@research.uwa.edu.au

Citation:
Salim, S., Pattiaratchi, C., Tinoco, R. O., & Jayaratne, R. (2018). Sediment resuspension due to near-bed turbulent effects: A deep sea case study on the northwest continental slope of Western Australia. *Journal of Geophysical Research: Oceans*, *123*. https://doi.org/10.1029/2018JC013819

Received 20 JAN 2018
Accepted 9 SEP 2018
Accepted article online 17 SEP 2018

Abstract Sediment transport equations often consider a mean velocity threshold for the initiation of sediment motion and resuspension, ignoring event-based turbulent *bursting* processes. However, laboratory experiments have suggested that near-bed sediment resuspension is influenced by intermittent turbulent coherent structures. In the field, accessibility constraints for deployment of easily operated equipment has largely prevented further identification and understanding of such processes, which may contribute to resuspension in the marine environment. Field experiments were conducted on the Northwest Slope, Australia, under conditions where the mean current velocities were below the estimated and measured time-averaged critical velocity to investigate the relationship between near-bed turbulent coherent structures and sediment resuspension. Results indicate that sediment resuspension occur even when velocities are below the estimated and measured mean critical values. The majority of turbulent sediment flux is due to ejection and sweep events, with lesser contributions from up-acceleration and down-deceleration (vertical flow) events. Spectral and quadrant analysis indicated the anisotropic and intermittent nature of Reynolds stresses, and wavelet transform revealed a group of turbulent bursting sequences associated with sediment resuspension. These observations, in flow conditions where resuspension was not expected to occur based on mean threshold concepts, reveal that intermittent turbulent events control sediment resuspension rather a single time-averaged critical velocity. This highlights the need of considering turbulence as a significant factor in sediment resuspension and should be further investigated for inclusion into future sediment transport modeling.

Plain Language Summary In this paper, investigation from deep-water (~375 m) field measurements were carried out, showing that in deep water conditions, fluid turbulent bursting phenomena plays a significant role in resuspending sediment, even for low-flow conditions under which transport equations (based on a time-averaged critical velocity) predict no transport. The finding of this study allows us advance the understanding of the near-bed sediment resuspension process for developing improved sediment transport equations and models in the future.

1. Introduction

1.1. The Role of Turbulence on Sediment Transport

Accurate knowledge of sediment transport mechanisms is crucial for a variety of problems ranging from river and coastal engineering to environmental science (Buffington, 1999; Kondolf et al., 2014; Mei et al., 1997; Robinson et al., 2005; Thompson et al., 2013; Wolanski et al., 2003). Despite extensive research in this field, including a large number of experimental studies (as detailed in Dey, 2011), the ability to estimate sediment transport is still hindered by a lack of understanding of all the physical processes contributing to sediment entrainment and resuspension (Aagaard & Jensen, 2013; Dwivedi et al., 2012). In this study, the term *resuspension* is used for particles initially on the seabed, which are eventually *lifted* into the water column, in contrast to particles permanently in suspension (i.e., washload). On the other hand, *entrainment* is used as the conditions just adequate to initiate sediment mobilization.

Most previous engineering and sedimentological applications have related sediment resuspension to a time-averaged bed shear stress. This concept suggests that sediment erodes and becomes resuspended when the bed shear stress exceeds a critical value (e.g., Shields, 1936). On the other hand, since the early

1950s, researchers attempted to characterize sediment entrainment advocating that it depended solely on fluid lifting force, with near-bed sediment being entrained due to instantaneous near-bed vertical velocity (Einstein, 1950; Ling, 1995; Velikanov, 1955). They reasoned that the sediment particles on the bed surface experience the maximum velocity gradient, and thus, a lift acts on the particles due to the pressure difference. Furthermore, they also conceptualized that the sediment particles may experience lift due to the instantaneous vertical velocity fluctuations in the vicinity of the bed and that the spinning motion of sediment particles may result in lift due to Magnus effect (Dey, 1999). Once the lift equals the submerged weight of the particle, a smaller force is necessary to entrain the bed particles. Other approach, as Wu and Chou (2003), studied the rolling and lifting probabilities for sediment entrainment, introducing the probabilistic features of the turbulent fluctuations and particle shape. Such probabilities were thus linked to threshold entrainment probabilities.

Kline et al. (1967) discovered a cyclical, nonperiodic process in fluids, a *turbulent bursting*, where the wall layer spreads slowly over a large period of time and then interacts strongly with the outer layer flow in an event-like manner. Bursting events involve a horseshoe or hairpin vortex, traveling centrifugally ejecting low-speed fluid away from the bed, experiencing a partial breakdown into turbulence ('ejection'). High-speed fluid can also move toward the bed (*sweep*). The vortex has transverse dimensions similar to the associated boundary layer streaks and keeps these general dimensions all over its lifespan (Allen, 1985; Wu & Shih, 2012). This discovery of the *bursting phenomenon* provided a new perspective to explore resuspension processes in turbulent flows.

Several laboratory studies established relationships between coherent motions within the turbulent boundary layer and sediment resuspension (Grass, 1974; Sumer & Deigaard, 1981; Sumer & Oguz, 1978; Sutherland, 1967). In a laboratory alluvial streambed, Sutherland (1967) noticed that sediment entrainment was result of the impact of a near-bed eddy onto the bed, producing a streamwise force able to mobilize the sediments. Grass (1974) investigated resuspension due to turbulent flow in strictly flat sand bed conditions, associating the ejection of fluid away from the boundary with the sediment response. Ejections conveyed a greater upward momentum flux of the particles than the downward flux and so were capable to resuspend particles denser than the fluid. Further laboratory studies using photographic techniques, Sumer and Oguz (1978), and Sumer and Deigaard (1981) detected that the uplifting of sediment particles was strongly controlled by ejections, and the process continued until the accompanying coherent structure breaks up, at which point particles begin to fall. While falling, a particle occasionally interacted with newly ejected fluid streaks due to other bursts, resulting in the particle rising again. These mechanisms kept occurring, continuously lifting particles into suspension. Falco (1991) experimentally noticed multiscale turbulent eddies in the inner-outer wall region and developed a coherent motion model. Focusing on a flat plate zero pressure gradient boundary layer, their study revealed that a particular set of coherent structures in the turbulent boundary layer were dynamically important for sediment motion. More recent experiments (Cellino & Lemmin, 2004; Kaftori et al., 1995; Mao, 2003; Nelson et al., 1995; Niño & Garcia, 1996; Salim et al., 2017) highlight the importance of turbulent bursting in laboratory conditions relating the ejections to sediment entrainment into the water column and sweep effectively transporting bedload (Cao, 1997; Dyer & Soulsby, 1988; Heathershaw, 1979; Keylock, 2007; Soulsby, 1983; Yuan et al., 2009).

Heathershaw and Thorne (1985) investigated the role of turbulent structures on sediment entrainment. Conducting experiments in tidal channels, they argued that entrainment was not correlated with the instantaneous Reynolds shear stress but with the near-wall instantaneous streamwise velocity. However, observations by Drake et al. (1988) on mobility of gravels in alluvial streams suggested that the majority of gravel entrainment was associated with sweep events giving rise to the motion of particles. These events occurred episodically during a small fraction of the time at any particular location on the bed. Thorne et al. (1989) observed that only sweeps and outward interactions played a significant role in the transport of coarse sedimentary material. It was the instantaneous increase in streamwise velocity fluctuations that generated excess boundary shear stresses in order to drive the transport process. In a microtidal saltmarsh channel, French and Clifford (1992) noticed that on average around 90% of the total intermittent Reynolds shear stress contributed to resuspend sediments for 50% of the total sampling time. Soulsby et al. (1994) demonstrated a significant link between the bursting process and the suspension of sediment within boundary layers. They made simultaneous measurements of the high-frequency fluctuations of sand concentration, resuspended in a tidal current, and the horizontal and vertical components of the water velocity above a sandy bed of an estuary.

They showed that large upward fluxes of sediment were associated with ejection events. Field experiments by Couturier et al. (2000) showed that the macroscale flow modules intensified the *ejection-like* turbulent events and sediment resuspension. *Ejection* events were associated with decreasing horizontal velocity and increasing turbidity, while *sweep* events were present during increasing horizontal velocity and decreasing sediment concentration. Yuan et al. (2009) conducted field experiments in the western Yellow Sea of China and suggested that the majority of turbulent sediment flux was the result of ejections and sweeps, while contributions from up-acceleration and down-deceleration events were significantly less.

Time-averaged bed shear stress threshold concepts for initiation of motion have long played a central role in sediment transport theory (e.g., since Shields, 1936). However, several investigations (e.g., Cellino & Lemmin, 2004; Mao, 2003; Niño & Garcia, 1996; Salim et al., 2017) reconsidered this concept and suggested that the turbulent bursting-based sediment entrainment has a major influence on sediment resuspension. For instance, Grass (1971) and Lavelle and Mofjeld (1987) concluded that based on empirical evidence, even at very low values of mean bed shear stress, turbulent fluctuations in instantaneous bottom shear stress as well as the random exposure of bed grains to the flow made it possible for particles to move. To our knowledge, limited field studies have been reported in this regard where mean flow speeds were below the time-averaged critical velocity. In one such investigation, O'Callaghan et al. (2010) examined the physical mechanisms underpinning sediment resuspension in the Swan River estuary, Western Australia, where mean currents were lower than critical levels but yet showed large turbidity events during intertidal oscillations. Similarly, experimental evidence conducted by Yang et al. (2016) in the shallow marine environment of southern Yellow Sea, China, suggested that the resuspension of sediment was related to intermittent turbulent events, where mean current velocity is lower than the predicted by existing threshold models.

1.2. Validation of Turbulent Bursting in the Deeper Ocean

Although field observations of turbulent coherent structures have been conducted regularly, field experiments with below-critical velocity conditions are relatively scarce (e.g., O'Callaghan et al., 2010; Yang et al., 2016; as mentioned above). To the best of our knowledge, no in situ observational studies in deep water conditions of the continental slope region has been performed to investigate the impact of bursting on below-critical flow fields, due to the lack of accessibility to the sites and availability of robust, easily operated deep water field equipment to measure turbulent velocity, and acoustic backscatter (as a surrogate measure of suspended sediment concentration [SSC]) simultaneously close to the seabed to estimate sediment resuspension. In the deep ocean systems (i.e., continental slope and continental shelf regions), engineers need to incorporate the influence of seabed mobility into the design of large scale marine infrastructure (e.g., platforms [rigs], subsea pipelines, jackets, and associated constructions such as subsea-mattresses and wellheads). However, consideration of the effect of near-bed turbulent coherent structures on sediment mobility (i.e., sediment entrainment and resuspension leading to erosion and scour) in the stability analysis of marine engineering structures are still elusive. The fluvial investigation conducted by Izadinia et al. (2013) on the stochastic nature of instantaneous shear stresses over the scour hole of hydraulic structures (in this case bridge piers) reported that the turbulent sweep events at the upstream side caused of maximum scour depth and led transportation of sediments to the downstream side. This further clarifies that the consideration of such commonly used transport models, which are based on time-averaged approaches, can increase the risk of insatiability of hydraulic structures. Furthermore, Leckie et al. (2016) suggested that in deep water systems (similar deployment locations as investigated in this paper), transport of sediment related to the subsea pipelines causes changes in benthic habitat conditions. Therefore, investigating turbulent bursting-based sediment transport process has significance for the better understanding of deep sea aquatic life.

All issues above are good reasons to explore the deep water systems of the continental slope and to investigate the influence of turbulent bursting on sediment transport. The aim of this paper is to describe the temporal and spatial relationships between the near-bed turbulent coherence structures and sediment resuspension in the continental slope region, in particular when mean velocities are below the estimated and measured mean critical velocities. In this study, the term *measured mean critical velocity* refers to a mean value determined by finding the velocity at which the recorded SSC was higher than the background level, as detailed in section 2.2 below. In situ observational study presented herein, at the southern end of the Australian Northwest Shelf provide a unique perspective to further understand the interactions between

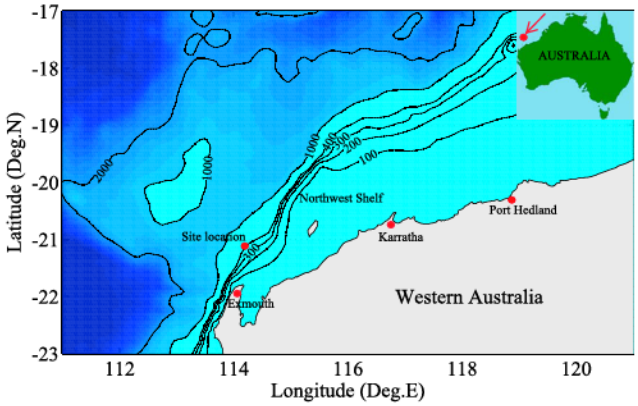

Figure 1. Bathymetric map of the Northwest Shelf showing the study site (red dot), located 53 km north-northwest of Exmouth in Van Gogh (−21° 23′51.63″N, 114° 04′04.89″E). contour lines represent water depth in meters.

sediment resuspension and turbulent characteristics on deep water conditions where measured and estimated (considering widely used transport equations) mean critical velocities are rarely exceeded.

The NW shelf region experiences strong semidiurnal tides (Holloway, 1983) with the tidal motion dominated by the principal lunar (M_2) and principal solar (S_2) constituents (Holloway, 1983). Spring tides can produce a range of over 6 m (Holloway, 1983), and these tides are the main forcing of currents in the bottom boundary layer on the continental shelf and slope (Katsumata, 2006) suggesting changes in current direction twice a day, consisting four slack tides per day. The bottom boundary layer currents speeds were up to 0.2 m/s (Holloway & Nye, 1985). The background ocean currents were also observed along the shelf where the main current ran counter to the anticlockwise flowing Eastern Boundary Current and flowed strongest away from the equator down the west coast of Western Australia during February–June. This unusual current is known as the Leeuwin Current and has maximum speed of approximately 0.25 m/s over the shelf break (Holloway & Nye, 1985). However, its influence on the bottom velocity currents is negligible compared to the tidal currents and internal currents as the Leeuwin Current weakens in association with persistently equatorward winds between September and January when the data presented in this paper was collected (Meuleners et al., 2007). The other influence on the shelf currents is internal waves (Antenucci & Ivey, 2006; Grant & Madsen, 1986; Nikora et al., 2002). Antenucci and Ivey (2006) found that large, local increases in energy levels gave peak speeds varying from 0.59 to 1.87 m/s for events lasting between 8 and 24 hr on the North West Cape in 302 m of water. These waves can cause the velocities to go beyond the threshold value for sediment resuspension but also cause turbulence, which can encourage the bursting phenomenon. Boegman and Ivey (2009) have shown that resuspension of sediment from shoaling internal waves was directly attributed to the near-bed viscous stress and near-bed patches of elevated positive Reynolds stress generated by the vertical structures. They also found that elevated near-bed viscous stresses were found throughout the domain at locations that were not correlated to the resuspension events, and that while these stresses were required for the sediment motion, it was not necessarily a precursor for resuspension (Boegman & Ivey, 2009), much like the results found for bursting (Robinson, 1991; Soulsby, 1983).

2. Study Area, Materials, and Methods

2.1. Site Description, Conditions, and Instrumentation

This study was an industry-based project, in collaboration with Apache Energy, an oil and gas company, using their remotely operated vehicles (ROVs) to deploy acoustic instrumentation on the seafloor. Data were collected from the southern end of the Northwest Shelf along the continental slope in 375-m water depth. The bathymetry at the site was gently sloping as the continental slope was quite wide in this location, and it was still in the transition stage, with only a small degree of slope. The instrument was deployed from a drilling rig located in the Van Gogh oil field (Figure 1) using a subsea ROV with real-time cameras and multifunctional arms (Figure 2).

A sediment core was taken during the deployment adjacent to the site location. Sieve analysis determined a mean particle size diameter d_{50} = 0.1 mm, sediment sorting coefficient S_o = 1.70, coefficient of gradation C_c = 1.3, and uniformity coefficient C_u = 6. Near the Van Gogh site, sediment samples were dominated by calcium carbonate ($CaCO_3$) deposited along a consistently flat terrain (AE, 2008; BHPB, 2012). These sediment classifications were consistent with previous investigations by Harris and Baker (1988). The drawback of taking measurements around the drilling rig was the presence of drill spoils, which came from drilling of the well, and the deployed instrument might have measured these drilling spoils as the sediment concentration. Therefore, the deployment location was carefully selected considering a more open area that had less spoils so that it did not affect the results of the typical sediment movement of the area.

Data were collected continuously for a 23-hr period starting at 15:00 on 26 September 2008, for a semidiurnal tidal cycle using a Nortek acoustic Doppler velocimeter (ADV) with titanium housing, rated to a depth of

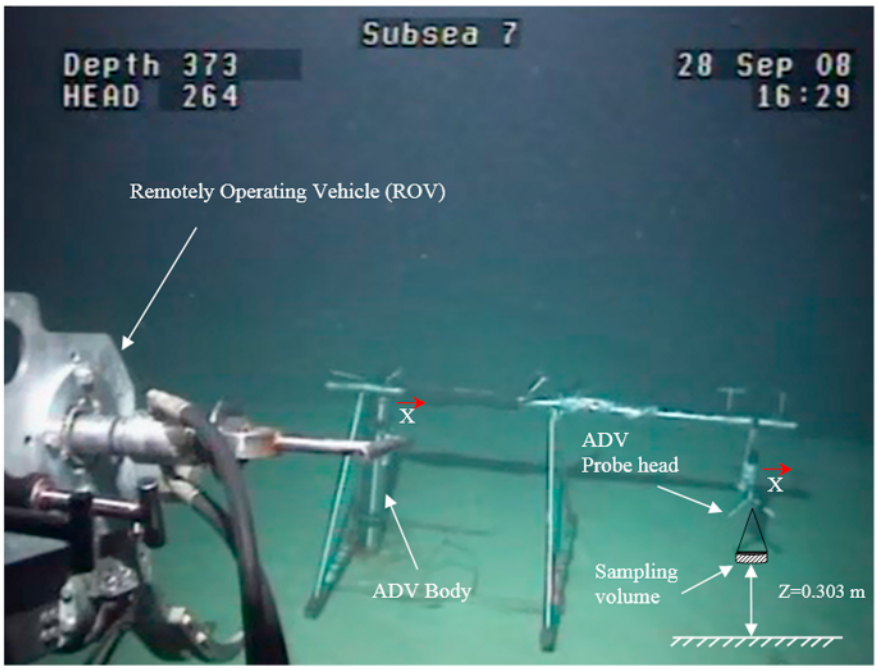

Figure 2. Real-time camera view showing the instrumental setup while remotely operated vehicle (ROV) extracting the instrument from the sea-floor (for better interpretation of "ROV extracting the instrument," interested readers can watch the video attached with the online version of this article).

3,000 m and a flexible head with a 2-m-long cable. The ADV was mounted looking downward to record the instantaneous velocities in ENU (East, North, Upwards) coordinates, posteriorly used to extract mean and turbulent velocity statistics, as well as synchronous backscatter eco intensity, used as a proxy for SSC, at a sampling rate of 8 Hz. The sampling volume of the ADV was located at 0.303 m above the seabed. The height was consistent throughout all measurements, as the recorded low currents did not change the dynamics of the visually observed flat bed, with no presence of bedforms nearby. Spectral frequency analysis found relevant frequencies in the system, yielding peaks in sediment suspension concentrations at corresponding peaks in the recorded velocities. Tidal prediction for the area was corroborated with temperature measurements taken by the ADV, as colder water from further down the continental slope, and warmer water from the coast are brought by tidal changes. These patterns were accompanied by strong temperature fluctuations indicating the interactions between tides and local currents.

2.2. Calculation of the Estimated and Measured Mean Threshold Velocity

The velocity threshold for initiation of motion at the deployment location (Van Gogh) was estimated using mean grain diameter (d_{50}) of 0.1 mm, a grain density (ρ_s) for Calcite ($CaCO_3$) of 2,710 kg/m^3 (Allen, 1985), and seawater density of 1,025 kg/m^3, using von Kármán constant as 0.41 and obtaining Nikuradse's roughness z_0 with

$$z_0 = \frac{k_s}{30}\left(1 - \exp\left[\frac{-u_* k_s}{27\upsilon}\right]\right) + \frac{\upsilon}{9u_*} \quad (1)$$

with $k_s = 2.5d_{50}$, $u_*$is the fluid friction velocity, and υ is the kinematic viscosity of water.

Based on widely used theoretical transport models such as Shields (1936), van Rijn (1984), Soulsby (1997), and Soulsby and Whitehouse (1997), the critical velocities for initiation of motion ranged between 0.281 and 0.679 m/s (Table 1). On the other hand, the measured mean critical velocity was determined in the field by tracking the changes in SSC and hydrodynamic conditions (Andersen et al., 2007; Shi et al., 2015), identifying the mean longitudinal (u) tidal velocity (i.e., main direction of the flow), turbulent kinetic energy (TKE) shear stress, and backscatter readings where sediment resuspension was just initiated. The *measured* critical

Table 1
Theoretical Mean Critical Values for Sediment Entrainment at z = 0.303 m Compared in This Study

Criteria	Equations	Estimated $\overline{u}_{cr}$ (m/s)
Shields (1936)	$\overline{u}_{\sigma} = \frac{u_*}{k}\ln\left(\frac{z}{z_0}\right)$ $u_* = \sqrt{[\theta_{cr}(s-1)gd_{50}]}$ θ_{cr} from Shields diagram $R_p = \frac{u_* d_{50}}{\nu}$ where s is specific gravity and u_* is fluid friction velocity.	0.302
van Rijn (1984)	$\overline{u}_{cr} = 0.19 d_{50}^{0.1}\log_{10}\left(\frac{4D}{d_{90}}\right); 100 < d_{50} < 500\ \mu m$ $\overline{u}_{\sigma} = 8.5 d_{50}^{0.6}\log_{10}\left(\frac{4D}{d_{90}}\right); 500 < d_{50} < 2{,}000\ \mu m$ where D is water depth and d_{50} and d_{90} are the corresponding percentiles on the granulometric curve.	0.520
Soulsby (1997)	$\overline{u}_{cr} = 7\left(\frac{D}{d_{50}}\right)^{1/7}[g(s-1)d_{50}f(D_*)]^{1/2}$ $s = \frac{\rho_s}{\rho} = \frac{\text{density of the sediment}}{\text{density of the fluid}}$ $D_* = \left[\frac{g(s-1)}{\nu^2}\right]^{1/3} d_{50}$ $f(D_*) = \frac{0.30}{1+1.2D_*} + 0.055\left(1 - e^{-0.020D_*}\right)$ for values of $D_* > 0.1$. where D_* is the dimensionless particle diameter	0.679
Soulsby and Whitehouse (Soulsby, 1997)	$\overline{u}_{\sigma} = \frac{u_*}{k}\ln\left(\frac{z}{z_0}\right)$ $u_* = \left(\frac{\tau_{cr}}{\rho}\right)^{1/2}$ $\tau_{cr} = \theta_{cr} g(\rho_s - \rho)d_{50}$ $\theta_{cr} = \frac{0.30}{1+1.2D_*} + 0.055\left(1 - e^{-0.020D_*}\right)$	0.281

velocity used in this paper represents a *time-averaged* value where the threshold was considered when ADV started recording the mean concentration higher than the mean background. The *measured mean critical velocity* is thus taken as the shift between the mean concentration from a baseline value to a clearly increased value.

2.3. Data Analysis

A set of 20 sections, 2-min long each, were analyzed in detail. Analysis focused on data with mean current velocity lower than the estimated and measured mean critical velocities. Prior to analysis, the data were split in 2-min segments, as is often done in this type of study to simplify the trends for visualization without losing any patterns (Kularatne & Pattiaratchi, 2008; Soulsby et al., 1994; Yang et al., 2016). Herein we present a detailed analysis of two such 2-min time series, between 91 to 93 min (TS-1), and 144 to 146 min (TS-2), as showed in Figure 3. Those two segments show the same patterns found throughout the whole time series (throughout the 20, 2-min series analyzed). An axis rotation algorithm based on principle component analysis was used along horizontal coordinates to transform the East (u velocity) component as the main direction of the flow for each section of the data (Emery & Thomson, 2001; Westra et al., 2010).

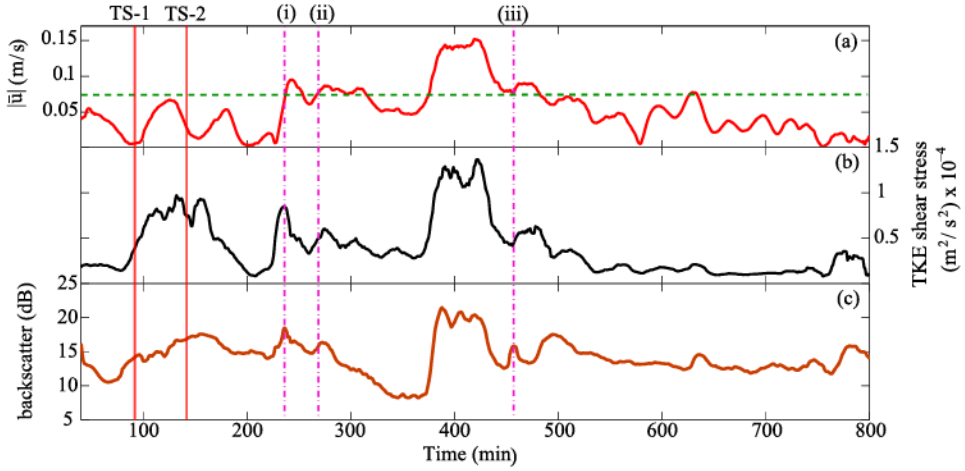

Figure 3. Time series between 40 and 800 min identifying events at (i), (ii), and (iii): (a) 1-min mean absolute *u*-directional velocity, (b) TKE bed shear stress, and (c) backscatter reading near the bed. The horizontal dashed line (green in color) showed the threshold resuspension velocity, and the vertical dashed lines (purple in color) showed the relevant seabed resuspension occurrence. Time Series-1 (TS-1) and Time Series-2 (TS-2) between 91 to 93 min and 144 to 146 min, respectively, are the segments (two- min long each) presented in this paper for detailed analysis.

2.3.1. Spectral Analysis

Spectral analysis (Figure 4) was conducted based on spectral energy cascade theory (Kolmogorov, 1941) for the three-dimensional inertial subrange spectrum:

$$E(k) = C_k \varepsilon^{2/3} k^{-5/3}, \tag{2}$$

where $E(k)$ is the energy spectrum based on the wave number; C_k is the Kolmogorov constant, deduced from experimental data (due to considerable uncertainty which lies between 1.4 and 2.2 as stated in Shalaby, 2007); ε is the rate of dissipation of energy; and k is the wave number (Baumert et al., 2005).

2.3.2. Reynolds Decomposition

Reynolds decomposition was used to determine the turbulent characteristics (Emery & Thomson, 2001; French & Clifford, 1992; Kularatne & Pattiaratchi, 2008):

$$u = \overline{u} + u', v = \overline{v} + v', w = \overline{w} + w', \tag{3}$$

where u, v, and w are the measured velocity components, primes denote instantaneous fluctuations, and overbars represent time averages. This decomposition allows calculation of the kinetic energy associated with turbulence, Reynolds shear stress, and inertial dissipation, as well as the assessment of the bursting phenomena. Due to the difficulty in identifying clear trends with the time series sampled at 8 Hz, we used a 1-s mean to facilitate analysis and identification without losing resolution. We estimated the turbulent integral time scale, as well as the Kolmogorov time scale of the time series presented in this paper, in order to ensure that sufficiently high temporal resolution was used for the investigation. For instance, for TS-1, integration of the autocorrelation function up to the first zero crossing (at $t = 0.375$ s) yielded a turbulent integral time scale of 0.09 s. On the other hand, considering the maximum velocity magnitude ($u_{max} = 0.089$ m/s) of the TS-1, we have estimated the Kolmogorov time scale based on the assumption that the dissipation rate is equal to the kinetic energy production rate at which kinetic energy supplied to the small scales (i.e., dissipation = $(u_{max})^3/L$, where L is the integral length scale, estimated as the product of the calculated integral time scale and a representative maximum velocity, u_{max}). Thus, we calculated the Kolmogorov time scale as 0.003 s, which is much lesser than the temporal resolution (i.e., 0.125 ≫ 0.003 s) of the data presented in this study. We also found the Kolmogorov time scale as 0.007 s considering as representative velocity the mean value (i.e., dissipation = $(u_{mean})^3/L$, where u_{mean} is a representative mean velocity magnitude), which is much lesser than the temporal resolution (i.e., 0.125 s ≫ 0.007 s) too. Similar time scales were found for TS-2. When compared to the turbulent integral time scale, our temporal resolution, 1/8 s, suggests that although we are not able to

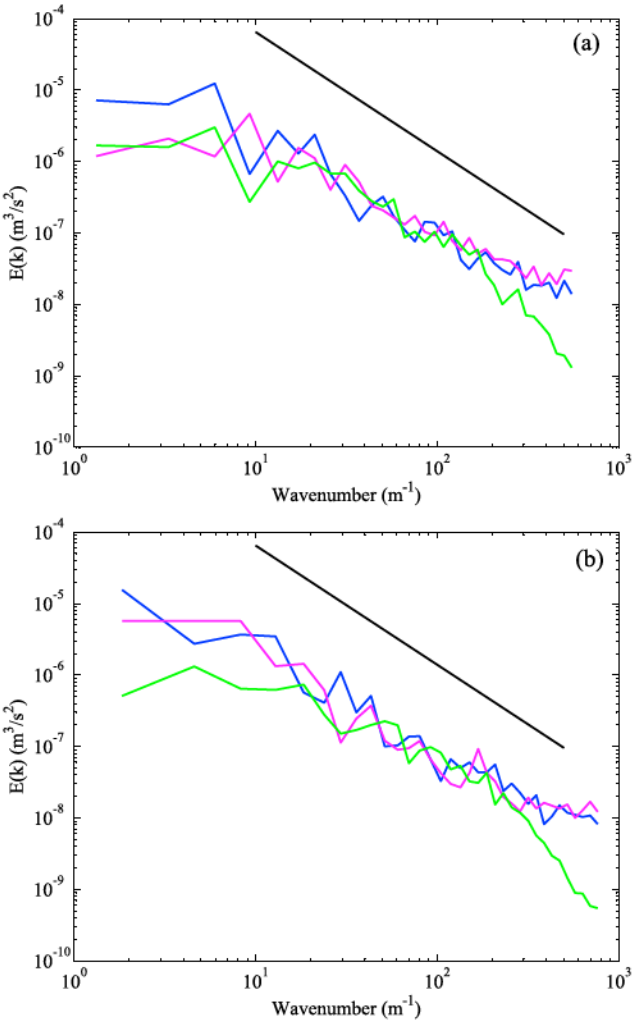

Figure 4. Wavenumber spectra of the velocity components between (a) 91–93 min (TS-1) and (b) 144–146 min (TS-2), where blue is the East component (*u*), magenta is the North component (*v*), and green is the vertical component (*w*). The solid line shows the −5/3 gradient of the energy dissipation equation.

resolve the fastest eddies from the recorded data due to the instrument limitations and deployment constrains in the deep water systems, our data resolution was able to capture most events, yielding adequate high temporal resolution for turbulence analysis.

2.3.3. Bed Shear Estimation

Single-point measurements of turbulent velocity fluctuations using ADV were used to calculate Reynolds shear stress (McLelland & Nicholas, 2000) widely used in previous field investigations (Couturier et al., 2000; Heathershaw, 1979; Kularatne & Pattiaratchi, 2008; Soulsby, 1983; Yuan et al., 2009). Stress values were estimated by

$$\tau_{Re} = -\rho\left(\overline{u'w'}\right), \tag{4}$$

where τ_{Re} is the Reynolds shear stress and ρ is the fluid density. Since, no quantitative analysis of Reynolds stress was undertaken, the term $u'w'$ represented turbulent Reynolds stress in this paper. Voulgaris and Trowbridge (1998) noticed that the ADV sensors can measure nearby Reynolds stress within 1% of the estimated true value. Kim et al. (2000) compared four different methods of bed shear stress estimations in the field at 0.440 m above the bed. They concluded that ADV sensors should be close enough to the bed but sufficiently far to avoid problems associated with velocity shear within the sampling volume. In line with other previous experiments in field conditions (e.g., Yuan et al., 2009, and Yang et al., 2016, who measured bottom stress at 0.450 and 0.500 m above the bed respectively), we determined measuring at 0.303 m above the bed as the optimum sensor height after several trials in order to avoid orientation problems and *weak spot* problem that caused interference and rendered the data to be unusable. Later in data analyzing stage, since the principle component analysis was used along horizontal coordinates to transform the East (*u* velocity) component as the main direction of the flow minimizing the transverse velocity (v velocity). Therefore, the $v'w'$ component was ignored in this study due to smaller values.

The TKE method, widely applied in oceanographic research (e.g., Biron et al., 2004), was used in calculating near-bed shear stress as

$$\mathrm{TKE} = 0.5\ \rho\left(\overline{u'^2} + \overline{v'^2} + \overline{w'^2}\right) \tag{5}$$

Since, no quantitative analysis of TKE stress was undertaken, the term ρ was ignored in this study.

As the ratio of TKE to the shear stress is constant, the measurement of shear stress was also used to estimate TKE-shear stress using the following equation (Pope et al., 2006):

$$\tau_{TKE} = 0.19\mathrm{TKE} \tag{6}$$

where τ_{TKE} is the TKE shear stress (Figure 5). Since the water density was considered constant in this study, therefore, the density of water was not presented for simplification.

2.3.4. Near-Bed Sediment Concentration Measurements

The ADV also records the reflection of the acoustic signal from particulate matter in water. Earlier studies (e.g., Fugate & Friedrichs, 2002; Voulgaris & Meyers, 2004) reported a simple logarithmic relationship between near-bed sediment concentration and backscatter index (derived as 10.log10[SSC]), however, in this investigation it was not practical to collect near-bed water samples due to large water depth (375 m) and difficulty of collecting near-bed water sample due to the limitation of instrumental facility. Particle size of the suspended sediment at the deployment location, d_{50} = 0.1 mm, falls within the detectable range of our ADV to use backscatter as a proxy for SSC (as discussed in Lohrmann, 2001). Given the below-critical conditions

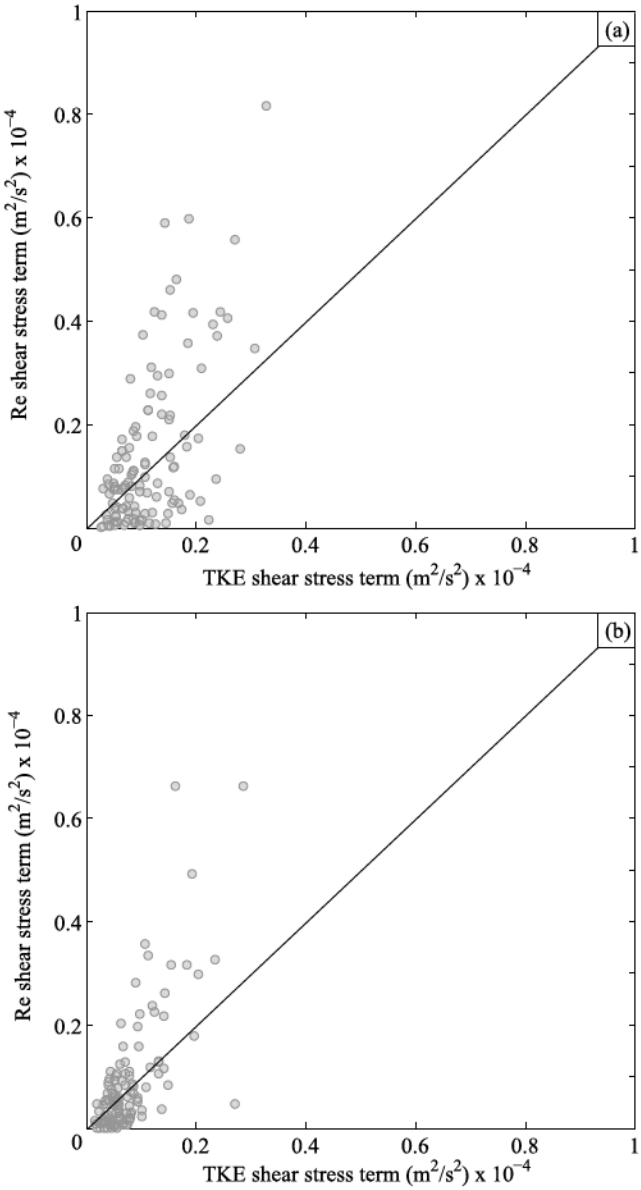

Figure 5. Comparison of the one-second mean Reynolds and turbulent kinetic energy (TKE) shear stresses within the selected two time series between (a) 91–93 min (TS-1) and (b) 144–146 min (TS-2). The solid black line defines the equality.

analyzed in this study, the SSC at the sampling location is not high enough to saturate the signal, allowing the use of recorded backscatter as proxy for SSC within the measured range. The following equation (Lohrmann, 2001) was used for the suspended particulate matter calculation:

$$EL = 0.43\ Amp + 20\log10\ (R) + 2\ \alpha_w\ R + 20R\int(\alpha_p dr), \quad (7)$$

where EL is the echo level in dB, Amp is the amplitude in counts recorded by the ADV, $R = 0.157$ is the range or distance between the transducer and focal point in meter, $\alpha_w = 0.7$ is the water absorption in dB/m (when salinity = 35 ppt for 1.5 MHz frequency, chosen from the list of values provided in Lohrmann, 2001), and α_p is the particle attenuation in dB/m. Lohrmann (2001) suggested that the particle attenuation becomes very small at low concentrations; therefore, the fourth term (i.e., $20R\int[\alpha_p dr]$) was ignored. Ejection and sweep events were identified using echo level (EL), considering the higher backscatter amplitudes produced by higher SSC. A concentration proxy (c') was also used as an indicator to identify variations in concentration of sediment, which was analyzed using Reynolds decomposition as discussed in Salim et al. (2017).

2.3.5. Quadrant Analysis

Quadrant analysis classifies different turbulent events and examines their intermittent nature and contribution to Reynolds stress. Kline et al. (1967) suggested the division of different burst motion events into u'-w' quadrants so that each event could be characterized and better understood based on their associated velocity fluctuations and their positions within the quadrant. It has become common to use quadrant analysis for studying intermittent turbulent structures and their contribution to sediment transport (e.g., Kularatne & Pattiaratchi, 2008; Yuan et al., 2009). Therefore, the statistics of velocity fluctuations (u' and w') were plotted in this study into quadrants on a u'-w' plane to study their significance (Liu et al., 2016; Lu & Willmarth, 1973). Such approach allowed us to identify the frequency of occurrence of each individual event within a bursting process as ejection ($u' < 0, w' > 0$), sweep ($u' > 0, w' < 0$), up-acceleration ($u' > 0, w' > 0$), and down-deceleration ($u' < 0, w' < 0$) (Izadinia et al., 2013; Kwoll et al., 2016). Recent work of Keylock et al. (2014) considered extending quadrant analysis into three dimensional octant analysis in order to characterize dominant flow structures, allowing linking to the sediment entrainment from the bed and into suspension, and the frequencies to dominate the velocity spectra contributing the majority of the total shear stress. However, u'-w' plane (a widely used two-dimensional quadrant approach) was chosen for this paper due to the simplicity of its implementation in exploring aspects of turbulent flow physics that otherwise have remained unidentified (Salim et al., 2017).

2.3.6. Wavelet Analysis

Wavelet analysis estimates the nonstationary power at many different frequencies of a time series (Daubechies, 1990). To reveal the dynamics of coherent structures and measure their contribution to the energy spectrum, continuous wavelet transform (CWT) was employed to derive the time evolution of momentum and sediment flux of turbulent coherent structures near the bottom boundary layer as described by Grinsted et al. (2004). Wavelet coherence (WTC) was also applied to expose regions with high common power showing phase relationships between the CWT of momentum and sediment flux. As the wavelet was not completely localized in time, the CWT and WTC edge artifacts were delimited in the power spectra by a cone of influence (COI). Therefore, results within the COI were avoided and visualized in the power spectra as a lighter shade. Further details of the applied algorithm and theory can be found in Grinsted et al. (2004).

3. Results

3.1. Tide and Temperature

In this study the history of tropical cyclones passing in the vicinity of the deployment location was reviewed and no storms of sufficient strength to create sediment mobility were noted. Tidal currents and solitons are, however, known to create strong water movements through this area (Baker et al., 2008). The tidal prediction for the area was compared to the temperature recorded by the ADV, which was used as a rough indication of the movement of water bodies. The temperature time series did not indicate the presence of internal waves during the measurement period.

3.2. Measurement of In-Situ Mean Critical Velocity

We identified the measured mean critical value using the records of backscatter and tidally induced mean velocity in the u direction. The near-bed backscatter showed significant increases (i.e., large spikes) in response to higher mean velocities on several occasions over shorts periods of time (events i, ii, and iii in Figure 3). The data indicated that the backscatter intensity, TKE shear stress, and mean velocity all had local maxima at (i) 236 min, (ii) 270 min, and (iii) 457 min, with the mean velocity reaching approximately 0.08 m/s (Figure 3). Earlier studies suggest that there is a background SSC within the water column (Van de Kreeke et al., 1997; Wang et al., 2009), likely due to the prevailing hydrodynamic conditions and the near-bed suspended sediment and inorganic matter with insufficient time to settle (Wang et al., 2009; Yang et al., 2016). Our field data indicated that background sediment concentration remained similar throughout the tidal cycle at the observation site. The measured mean critical velocity is thus determined for this study as 0.08 m/s. It should be noted that the estimated critical velocities (Table 1) were higher than the measured values that corresponded to a detectable increase in sediment concentration (increase in the mean SSC); therefore, the observed values are more appropriate to define the *threshold* condition of motion. Indeed, using transport equations to define critical velocities (e.g., Pattiaratchi & Collins, 1985) may not attain the strictly defined entrainment conditions but, instead, referring to a small amount of transport above the threshold condition of motion (Buffington, 1999).

3.3. Spectral Analysis of Turbulence

Time series of turbulent velocities were used to obtain the frequency (f) spectra, then converted to wave number (k) spectra following Taylor's *frozen turbulence* hypothesis (Soulsby, 1983). The velocity spectra exhibited general agreement with the $-5/3$ slope in the inertial subrange (Taylor, 1938), in the wide range of $20 < k < 200$/m and $30 < k < 200$/m for time series TS-1 and TS-2, respectively (Figure 4). This range was obtained through direct comparison of the $-5/3$ gradient of the energy dissipation equation (black solid lines in Figure 4) with the three velocity components (i.e., u', v', and w'). We also discarded the signal beyond this range due to instrumental noise (Voulgaris & Trowbridge, 1998). In more details, the inertial subrange spectral slope for the case of TS-1 was observed as 1.25 (~5/4) for u, 1.25 (~5/4) for v, and 1.67 (~5/3) for w (Figure 4a). For TS-2 the inertial subrange spectral slope was 1.67 (~5/3) for u, 1.25 (~5/4) for v, and 1.25 (~5/4) for w (Figure 4b). The presence of *inertial subrange* in both time series confirmed the existence of turbulent structures dominating the TKE transfer process at the deployment location where the motions were governed by the inertial effects with viscous effects negligible (Ferziger, 2005). The $-5/3$ spectral slope in measurements close to the seabed is not common (George et al., 1994; Hino et al., 1983; Kularatne & Pattiaratchi, 2008; Smyth & Hay, 2003) since the closer to the seabed, the less steep the slope of vertical velocity spectra in the inertial subrange (Smyth & Hay, 2003). The observed spectral results consistently determined the existence of the inertial subrange in the rest of the data set, which provided confidence for further analysis of small eddy turbulent coherent structures.

3.4. Bed Shear Stress Estimates

The scatterplot of bottom shear stress term between TKE and Reynolds methods for the two time series (TS-1 and TS-2) indicates that intermittent higher shear stress (i.e., TKE- and Re-shear stress term estimations of both TS-1 and TS-2 runs; grey dots in Figure 5) result in sediment resuspension (backscatter intensity on Figures 6 and 7, respectively). Biron et al. (2004) suggested that in a simple turbulent boundary layer, the TKE estimates were systematically lower than Reynolds estimates at high stress level. Comparing the two shear stress calculations, they do not present a clear 1:1 equivalence. A clear deviation toward the Re shear stress is noticed, specially for values greater than 0.2×10^{-4} m^2/s^2 in TKE- and Re-shear stress term

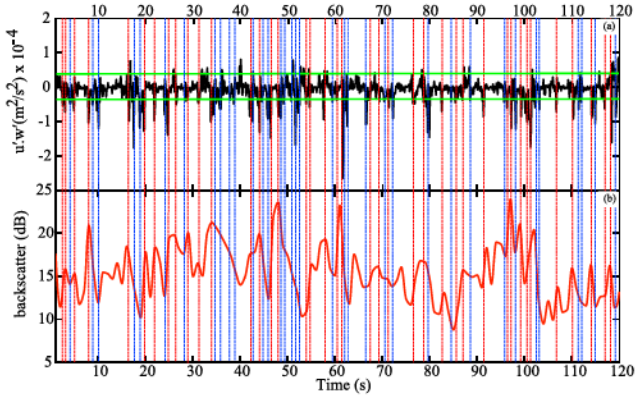

Figure 6. Time series records of the selected 2-min period between 91 and 93 min (TS-1) where $\bar{u}$ (0.039 m/s) < $\bar{u}_{cr,\ measured}$ (0.080 m/s): (a) turbulent Re shear stress ($u'w'$), showing ejection (red dotted lines) and sweep (blue dotted lines) events, and (b) 1-s mean of the backscatter. The horizontal green solid line shows the 1 standard deviation criterion to identify the major ejection and sweep events.

estimations (Figure 5), which is in general quantitative agreement with results from Biron et al. (2004). For single-point measurements, Heathershaw (1979) suggested that the near-bed value of Re shear stress provided better estimation of the highly intermittent nature of turbulence. Hence, Reynolds shear stress was chosen for further investigation.

3.5. Comparison of the Raw Time Series

The trends in Reynolds shear stress and backscatter were examined. The mean current velocity was $\bar{u}$ = 0.039 m/s, 48.75% of the measured time-averaged critical velocity ($\bar{u}_{cr}$ = 0.08 m/s) for TS-1 (Figure 6). Overall ejection and sweep events occurred marginally more often than up-acceleration and down-deceleration events, resulting in a larger contribution to momentum and sediment fluxes. We considered the major ejection and sweep events as values greater than 1 standard deviation of the Reynolds stress term ($u'w'$) for both time series presented in this paper (i.e., for TS-1: $u'w' > 3.41 \times 10^{-05}$ m^2/s^2 and for TS-2: $u'w' > 2.52 \times 10^{-05}$ m^2/s^2), which allowed us to investigate the extreme ejection and sweep events that falls in the 31.8% of the total Re shear stress term of the time series. In TS-1, 75 major ejection and sweep events were analyzed in detail, identifying 39 events during ejections and 36 during sweeps as shown in Figure 6. Similarly, in TS-2 where the mean current velocity ($\bar{u}$ = 0.028 m/s) was 35% of the measured time-averaged critical velocity ($\bar{u}_{cr}$ = 0.08 m/s), 57 major ejection and sweep events were analyzed in detail, identifying 33 events during ejections and 24 during sweeps (Figure 7). Both time series showed that high-resuspension events (i.e., backscatter reading showed changes greater than 1 dB in compare to background concentration) below the measured time-averaged critical velocity were associated with major ejections and sweeps, which was consistent with all the 20 sections investigated. In the deep water field conditions of the continental slope, identification of such resuspension events due to turbulent bursting, particularly ejections and sweeps, supports the argument of the nonexistence of a mean critical velocity, as results further indicate that although flow conditions were below the measured mean critical velocity conditions, sediment resuspension was observed due to ejection and sweep events.

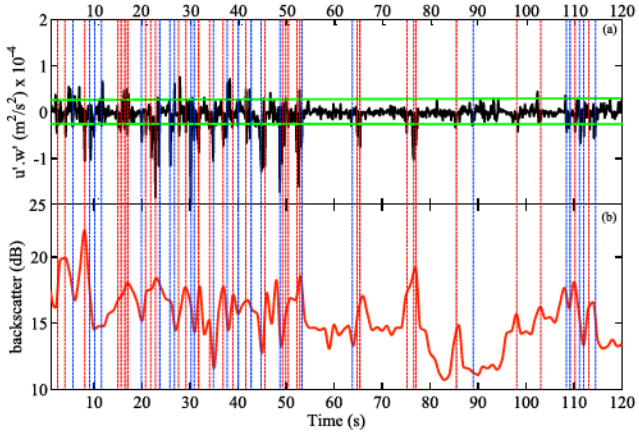

Figure 7. Time series records of the selected 2-min period between 144 and 146 min (TS-2) where $\bar{u}$ (0.028 m/s) < $\bar{u}_{cr,\ measured}$ (0.080 m/s): (a) turbulent Re shear stress ($u'w'$), showing ejection (red dotted lines) and sweep (blue dotted lines) events, and (b) 1-s mean of the backscatter. The horizontal green solid line shows the 1 standard deviation criterion to identify the major ejection and sweep events.

3.6. Statistical and Quadrant Analysis

The contributions of $u'w'$ from the selected 2-min periods were separated into the four quadrants of the u'-w' plane (Figures 8a and 8b). Both figures showed a clear lack of large contributions in up-acceleration and down-deceleration when compared to ejections and sweeps. The scattering of turbulent components in the u'-w' plane below the time-averaged measured critical velocity was consistent in the whole data set. Such a distribution of turbulent components in the u'-w' plane established that ejection and sweep events can occur even below a measured mean critical threshold value in deep sea conditions.

Quadrant analysis was used to quantitatively evaluate the intermittency and determine the contributions of the four kinds of bursting events to the Reynolds stress for TS-2 as a representation of the 20 data sets (Figure 9). Below the measured mean critical velocity, it was observed that ejections and sweeps were the dominant sources of Reynolds stress generation. Time of occurrence, net Reynolds shear stress, and sediment flux by ejections (30, 38, and 33%, respectively) were near equivalent with sweeps (27, 33, and 29%, respectively), while the up-acceleration and down-deceleration events made significantly less contributions to all three cases. Histograms (Figure 9) showed that the upward sediment flux was prominently accomplished by ejections (38%) and sweeps (33%), suggesting that intense surge of low-speed fluid containing high sediment

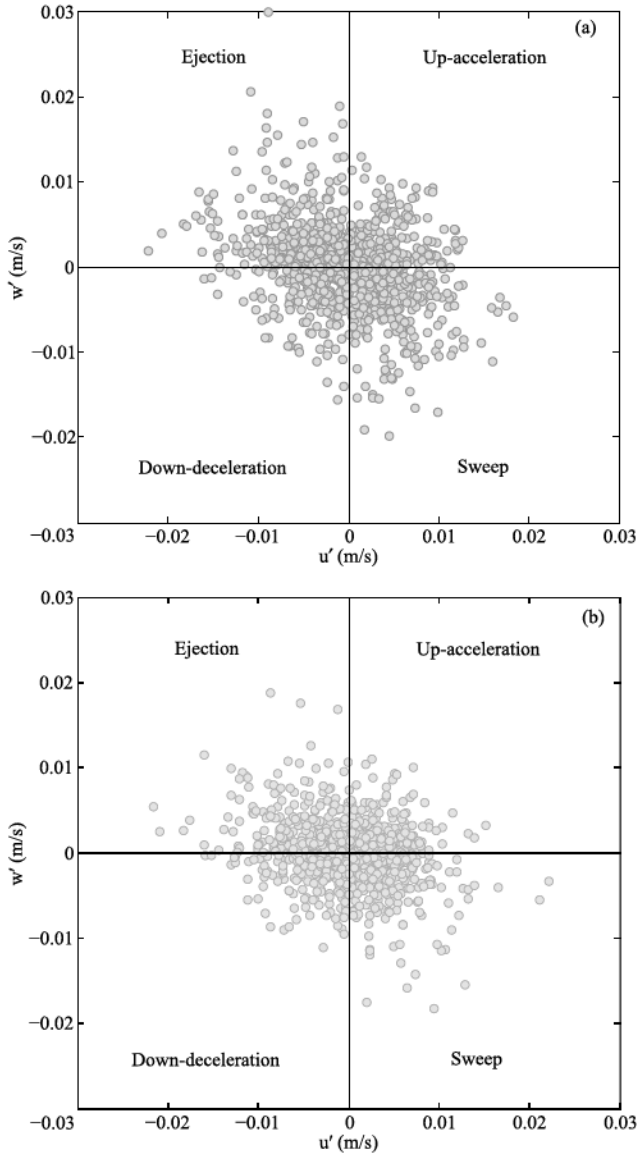

Figure 8. Classification of bursting events in u'-w' space mentioning ejection, sweep, up-acceleration, and down-declaration of the selected time series between (a) 91–93 min (TS-1) and (b) 144–146 min (TS-2) where red and grey dots for values above and below the thresholds, respectively.

concentration and high speed fluid rushing toward the bed was the main provider of $c'w'$ (i.e., ejection = 33% and sweep = 29% in sediment flux). Up-acceleration (19%) and down-deceleration (19%) events transported significantly less sediment. Collectively, turbulent sediment flux primarily occurred as a result of ejections and sweeps (62%), with a smaller contribution from up-acceleration and down-deceleration events (38%).

3.7. Wavelet Analysis of Reynolds Stresses and Sediment Resuspension

CWT and WTC were performed with 8 Hz sampling rate over the selected two time series of TS-1 and TS-2 (Figures 10 and 11). In the scalograms, the white-shaded region represents the COI where the image might be distorted due to edge effects limiting the capability to investigate the lower frequencies (see section 2.3.6). Hence, we limited the investigation to examine low-frequency events occurring lower than 0.0313 Hz.

In general, the results of the two presented time series (TS-1 and TS-2) tracked the hydrodynamics of turbulent coherent structures and associated measured contribution to the sediment flux. Data revealed that within the large-scale motions (considering frequency bands <0.5 Hz as large-scale motions), there existed multiscale features. For instance, (1) in TS-1 of approximately 61–64 s, frequency band is approximately 0.125–0.5 Hz (large scale) and approximately 1–2 Hz (small scale), and (2) in TS-2 of approximately 41–44 s, frequency band is approximately 0.125–1 Hz (large scale) and approximately 1–2 Hz (small scale).

It also exhibited some embedding small fine-scale features. For example, (1) in TS-1 at approximately 22–25 s, frequency band is approximately 1–2 Hz and (2) in TS-2 at approximately 21–24 s, frequency band is approximately 1–2 Hz) features.

These indicates that for both TS-1 and TS-2 near the bed, most of the energy was concentrated within the high wavelet power zones (i.e., warmer color >0.5 s) in momentum flux and sediment flux scalograms. The presence of such multiscale and small-scale features within large-scale motions also revealed the random nature of background turbulence where, with the decreasing values of frequencies, the wavelet contours appeared to be well organized.

The comparison of high-energy wavelet power zones (i.e., warmer color, >0.5 s) and high-frequency turbulent events also confirmed the intermittent nature of turbulence throughout the records (e.g., indicated major

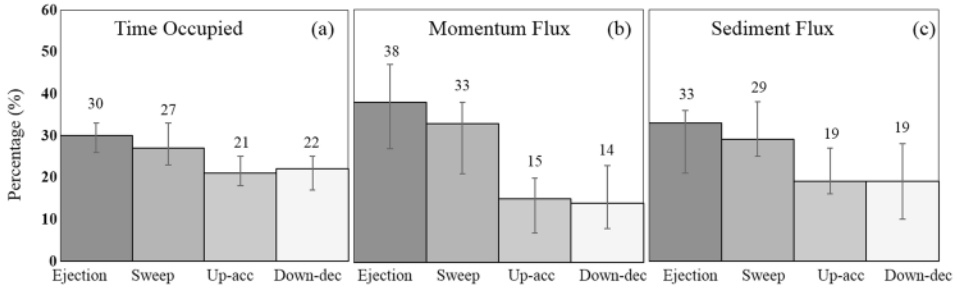

Figure 9. Quadrant analysis of coherent structures of the selected 2-min period between 91 to 93 min (TS-2, where $\bar{u} < \bar{u}_{cr,measured}$) showing the (a) time occupied, (b) momentum flux ($u'w'$), and (c) sediment flux ($c'w'$). The error bars represent the maximum and minimum values of the analyzed total data set (twenty 2-min long sections).

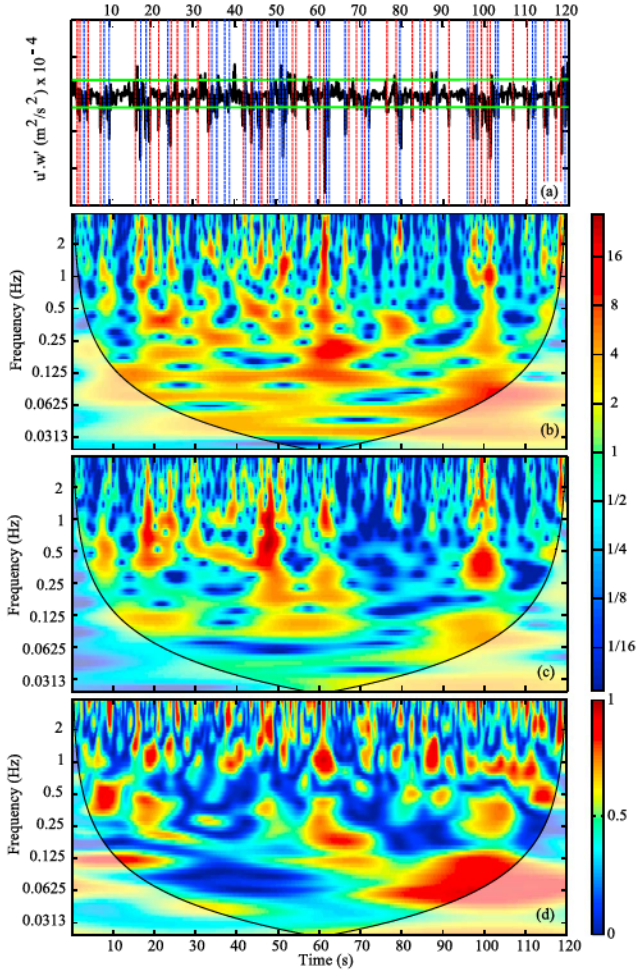

Figure 10. Squared wavelet coherence of the TS-1 between 91 and 93 min (where $\bar{u} < \bar{u}_{cr}$) showing the (a) turbulent Re shear stress ($u'w'$), showing ejection (red dotted lines) and sweep (blue dotted lines) events (b) momentum flux ($u'w'$), (c) sediment flux ($c'w'$), and (d) coherence between the momentum and sediment fluxes.

ejection and sweep events in TS-1 and TS-2 of Figures 10a and 11a respectively).

We also noticed that the major ejection and sweep events (i.e., as indicated in Figures 10a and 11a) at lower frequency bands (~0.033–0.25 Hz in both Figures 10b and 10c and 11b and 11c), which lasted for a longer time (i.e., taking >3 s time), contributed largely to transport sediments before fading as shown in Figures 10c and 11c, respectively. These emphasized that not only magnitude but duration of these turbulent forces contributes to the sediment flux.

The WTC was applied to turbulent fluctuations of momentum and sediment flux where shared features were observed (Figures 10c and 11c in relation to the indicated ejection and sweep events in Figures 10a and 11a). Resuspension events and turbulent stresses at a range of scales exhibited high common power (i.e., warmer color >0.5). For instance, the major ejection and sweep events identified between 97 and 101 s in the TS-1 (Figure 10c) revealed a higher correlation between momentum and sediment flux (i.e., warmer color >0.5 s) with the frequency band ranging between ~0.5 and 2 Hz. At smaller frequencies, these regions of significant common power occurred near the bed for a majority of the time. Consistently, in both TS-1 and TS-2, the larger groups fell over short bands of frequency scales (predominantly 0.03125 and 0.25 s), while the rapidly evolving bands (considering those lasting >3 s) spread over a larger range of frequency scales (primarily between 0.0313 and 0.25 Hz) before fading. This was evident in the color-coded contours (Figures 10d and 11d with corresponding major ejection and sweep events) where momentum flux corresponded to the contour in sediment flux within similar frequency bands. Such results were also observed in the remaining data set.

3.8. Intercomparison of Threshold Approaches

An intercomparison between widely used sediment motion criteria (Shields, 1936; Soulsby, 1997; Soulsby & Whitehouse, 1997; van Rijn, 1984; primarily derived from Shields diagram) and measured mean critical velocity was undertaken to examine the validity of threshold predictors in the deeper ocean (water depths ~375 m). The measured mean critical velocity was clearly below the estimated Shields (1936), van Rijn (1984), Soulsby (1997), and Soulsby and Whitehouse (1997) threshold values (i.e., 0.08 m/s < 0.302, Shields, 1936; 0.520 m/s, van Rijn, 1984; 0.679 m/s, Soulsby, 1997; and 0.281 m/s, Soulsby & Whitehouse, 1997). This indicated that the well-known empirical methods, which are well established for the practical engineering design of movable-bed channels, potentially indicate no resuspension at the subthreshold conditions, while the measured SSC mostly indicated otherwise.

4. Discussion

Previous studies (Lavelle & Mofjeld, 1987; Niño et al., 2003; Niño & Garcia, 1996) suggested the nonexistence of a true threshold for sediment motion. This issue was explored in Salim et al. (2017) through the analysis of high-resolution (50 Hz) acoustic data in laboratory conditions and provided evidence for resuspension of sediments below the time-averaged measured and estimated critical velocities. However, such fluvial studies of turbulence and sediment transport require to consider the effect of flow geometry, which may induce artefact hydrodynamics causing significant influence on the processes being investigated. Therefore, despite previous laboratory-based investigations (e.g., Salim et al., 2017), field investigations reported in this study was required to clearly understand the role of coherent structures on sediment resuspension below the calculated and measured time-averaged critical velocity conditions and validate laboratory findings. Results presented in this paper, clearly establish the argument that both ejection and sweep events contribute to momentum flux as well as sediment flux in a deep water environment where both the measured and

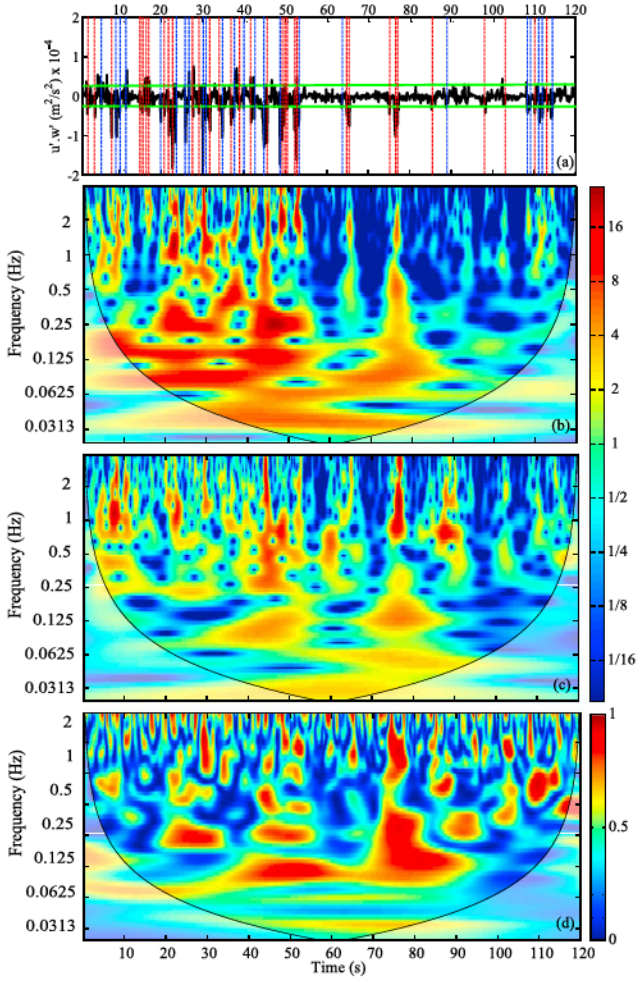

Figure 11. As Figure 10 but for TS-2 between 144 and 146 min.

calculated critical velocity rarely exceeded. Our study shows that the concept of time-averaged critical velocity by itself cannot provide a full representation of the physical processes in sediment resuspension. The observed dependence of sediment resuspension on turbulent bursting events (in particular, ejections and sweeps) below time-averaged critical velocity conditions raises fundamental questions concerning theoretical predictions of sediment transport in deep water conditions, requiring the development of a new generation of turbulence incorporated transport models.

Researchers have presented laboratory and field evidence supporting the close correlation between the instantaneous sediment flux and instantaneous streamwise velocity (u), suggesting that only sweeps and up-accelerations play a significant role in the entrainment and transport of sediment, since these motions were associated with positive u' and thus greater streamwise velocities (Nelson et al., 1995; Thorne et al., 1989; Weaver and Wiggs, 2008). In this study the estimated and measured time-averaged critical velocities in natural flow conditions observed that ejection and sweep events strongly dominated over up-acceleration and down-deceleration events (Figures 8a and 8b). While previous investigations (e.g., Heathershaw & Thorne, 1985; Nelson et al., 1995; Thorne et al., 1989) found that up-acceleration and down-deceleration events considerably contributed to sediment resuspension, our investigation showed lower net sediment fluxes were associated with such events. Our results obtained in conditions below time-averaged critical velocity conditions agrees with other research, which have documented that sweeps and ejections were the primary contributors to sediment entrainment (Best, 1992; Grass, 1971, 1974; Hurther & Lemmin, 2003; Niño & Garcia, 1996; Sumer & Deigaard, 1981). It should be noted that our sampling volume was placed at a higher level above the bed (i.e. 0.303 m), and weaker up-acceleration and down-deceleration events might not have carried sediment particles to such an elevation. Still, in our measurements, up-acceleration and down-deceleration events contributed less effectively.

Wavelet analysis provided a complementary approach to the traditional Fourier spectrum analysis diagnosing characteristics of turbulence in order to explain information about the spatial structure of the flow. Particularly, we were interested in its frequency content and energy variation (Figures 10 and 11). The time series TS-1 and TS-2 through wavelet analysis indicated that clusters of low-frequency coherent flow structures were initiated close to the bed, which were closely followed by periods of powerful resuspensions near the bed, emerging from the integral scales, and decaying with time, after the termination of the turbulent agitation. In agreement with laboratory work of Driver et al. (1987) and Simpson (1989), that indicated the frequency at which coherent structures were generated, our study revealed that at higher frequencies the intermittent and relatively large momentum regions exhibited a direct role in resuspension of sediment. In the outer boundary layer region, turbulent fluctuations were dominant in driving and maintaining high-frequency resuspensions as long as momentum was supplied. Such wavelet-based analysis has not been applied to data from deep water systems, also validate the argument of Salim et al. (2017) and Yuan et al. (2009), where investigation was carried out in laboratory and shallow water tidal current environments. Therefore, it can be stated that the cross wavelet transform method was effective at visualizing and detecting the coherent structures from the raw turbulent data, which enabled us to study the correlation between wall turbulence structures and sediment resuspension.

5. Conclusions

A complete understanding of sediment transport will improve design of marine infrastructure, reducing the risk factor of underestimating sediment transport rates. The uniqueness of this study is that particle

micromechanics were examined in terms of turbulent bursting features under deep water conditions where the mean current velocity was low. In particular, it was shown that each turbulent event, relative to the time frame of measurement contributed to the suspension process below the mean critical velocity conditions. Our results showed consistency with laboratory studies (e.g., Salim et al., 2017) where the mean current flow was below the measured mean critical velocity conditions. Quadrant analysis suggested that in agreement with previous laboratory and field experiments, sediment flux was largely controlled by ejections and sweeps. Instantaneous particle entrainment occurred earlier than the suggested measured time-averaged critical velocity due to the stochastic nature of turbulence. Wavelet analysis revealed signatures of correlation between wall turbulent structures and sediment resuspension. Over time, turbulence occurred in slowly evolving clusters that were closely followed by periods of high resuspension events near the bed, evolving from the primary leading scales toward low frequencies and decaying in time after the termination of the turbulent event. While sediment resuspension is related to a single time-averaged value of critical shear stress, our quadrant and wavelet-based analysis highlights the importance of the turbulent bursting concept and suggests to incorporate it in future transport models, which will contribute toward sediment resuspension in scenarios well below the average critical threshold.

Acknowledgments
This work was part of the first author's PhD research supported by the Scholarship for International Research Fees (SIRF), University International Stipend (UIS), and Safety Net Top-Up Scholarship awarded by the UWA Oceans Institute and School of Civil Environmental and Mining Engineering at the University of Western Australia. We sincerely extend our gratitude to Kate Swain for her contribution in collecting the data set. Thanks to the South-East Asian Scientific and Environmental ROV Partnership using Existing INdustrial Technology (SEA SERPENT) project for providing the facilities to collect the data. Funding for data collection was provided by the Australian Research Council (ARC) Linkage Grant LP0775183, which was supported by, Santos, and Woodside Energy. Data presented in this manuscript are available online at FigShare repository, at https://figshare.com/articles/Data_mat/7001096.

References

Aagaard, T., & Jensen, S. G. (2013). Sediment concentration and vertical mixing under b reaking waves. *Marine Geology*, *336*, 146–159. https://doi.org/10.1016/j.margeo.2012.11.015

AE (2008). *Van Gogh Oil Field Development*. Perth: Apache Energy Limited.

Allen, J. R. L. (1985). Order in chaos. In *Principles of physical sedimentology* (pp. 103–122). Dordrecht, Netherlands: Springer. https://doi.org/10.1007/978-94-010-9683-6_6

Andersen, T. J., Fredsoe, J., & Pejrup, M. (2007). In situ estimation of erosion and deposition thresholds by Acoustic Doppler Velocimeter (ADV), Estuarine. *Coastal Shelf Science*, *75*(3), 327–336. https://doi.org/10.1016/j.ecss.2007.04.039

Antenucci, J. P., & Ivey, G. N. (2006). Observations of bottom intenisfication of temperature and velocity fluctuations induced by oblique tidal interactions with a slope. *Marine and Freshwater Research*, *57*(3), 255–263. https://doi.org/10.1071/MF05054

Baker, C., Potter, A., Tran, M., & Heap, A. D. (2008). Geomorphology and Sedimentology of the Northwest Marine Region of Australia. Geoscience Australia, Record 2008/07 (220 pp.). Canberra: Geoscience Australia.

Baumert, H. Z., Simpson, J. H., Sundermann, J. (Eds.) (2005). *Marine turbulence: Theories, observations and models. Results of the CARTUM Project*. Cambridge: Cambridge University Press.

Best, J. l. M. (1992). On the entrainment of sediment and initiation of bed defects: Insights from recent developments within turbulent boundary layer research. *Sedimentology*, *39*(5), 797–811. https://doi.org/10.1111/j.1365-3091.1992.tb02154.x

BHPB (2012). Pyrenees expansion tophole environment plan summary, BHP Billiton Petroleum Pty Ltd, 2012.

Biron, P. M., Robson, C., Lapointe, M. F., & Gaskin, S. J. (2004). Comparing different methods of bed shear stress estimates in simple and complex flow fields. *Earth Surface Processes and Landforms*, *29*, 1403–1415. https://doi.org/10.1002/esp.1111(11)

Boegman, L., & Ivey, G. N. (2009). Flow separation and resuspension beneath shoaling nonlinear internal waves. *Journal of Geophysical Research*, *114*, C02018. https://doi.org/10.1029/2007JC004411

Buffington, J. M. (1999). The legend of A. F. Shields. *Journal of Hydraulic Engineering*, *125*(4), 376–387. https://doi.org/10.1061/(ASCE)0733-9429(1999)

Cao, Z. (1997). Turbulent bursting-based sediment entrainment function. *Journal of Hydraulic Engineering*, *123*(3), 233–236. https://doi.org/10.1061/(ASCE)0733-9429(1997)123:3(233)

Cellino, M., & Lemmin, U. (2004). Influence of coherent flow structures on the dynamics of suspended sediment transport in open-channel flow. *Journal of Hydraulic Engineering*, *130*(11), 1077–1088. https://doi.org/10.1061/(ASCE)0733-9429(2004)

Couturier, M. N. L., Grochowski, N. T., Heathershaw, A., Oikonomou, E., & Collins, M. B. (2000). Turbulent and macro-turbulent structures developed in the benthic boundary layer downstream of topographic features. *Estuarine Coastal Shelf Science*, *50*(6), 817–833. https://doi.org/10.1006/ecss.1999.0602

Daubechies, I. (1990). The wavelet transform, time–frequency localization and signal analysis. *IEEE Transaction on Information Theory*, *36*(5), 961–1005. https://doi.org/10.1109/18.57199

Dey, S. (1999). Sediment threshold. *Applied Mathematical Modelling*, *23*(5), 399–417.

Dey, S. (2011). Entrainment Threshold of Loose Boundary Streams. In P. Rowinski (Ed.), *Experimental methods in hydraulic research* (pp. 29–48). Berlin, Heidelberg: Springer.

Drake, T. G., Shreve, R. L., Dietrich, W. E., Whiting, P. J., & Leopold, L. B. (1988). Bedload transport of fine gravel observed by motion-picture photography. *Journal of Fluid Mechanics*, *192*, 193–217. https://doi.org/10.1017/S0022112088001831

Driver, D. M., Seegmiller, H. L., & Marvin, J. G. (1987). Time dependent behavior of a reattachment shear layer. *American Institute of Aeronautics and Astronautics Journal*, *25*(7), 914–919. https://doi.org/10.2514/3.9722

Dwivedi, A., Melville, B., Raudkivi, A., Shamseldin, A., & Chiew, Y. (2012). Role of turbulence and particle exposure on entrainment of large spherical particles in flows with low relative submergence. *Journal of Hydraulic Engineering*, *138*(12), 1022–1030, https://doi.org/10.1061/(ASCE)HY.1943-7900.0000632

Dyer, K. R., & Soulsby, R. L. (1988). Sand transport on the continental shelf. *Annual Review of Fluid Mechanics.*, *20*(1), 295–324. https://doi.org/10.1146/annurev.fl.20.010188.001455

Einstein, H. A. (1950). *The bed-load function for sediment transportation in open channel flows. US Department of Agriculture* (Vol. 1026). Washington DC: Technical bulletin number.

Emery, W. J., & Thomson, R. E. (2001). Chapter 4 - the spatial analyses of data fields. In *Data analysis methods in physical oceanography* (pp. 305–370). Amsterdam: Elsevier Science.

Falco, R. E. (1991). A coherent structure model of the turbulent boundary layer and its ability to predict Reynolds number dependence. *Philosophical Transactions: Physical Sciences and Enineering*, *336*(1641), 103–129.

Ferziger, J. (2005). Turbulence: its origins and structure. In H. Z. Baumert, J. H. Simpson, & J. Sundermann (Eds.), *Marine turbulence: Theories, observations and models* (pp. 4–13). Cambridge: Cambridge University Press.

French, J. R., & Clifford, N. J. (1992). Characteristics and 'event-structure' of near-bed turbulence in a macrotidal saltmarsh channel. *Estuarine, Coastal and Shelf Science*, *34*, 49–69. https://doi.org/10.1016/S0272-7714(05)80126-X

Fugate, D. C., & Friedrichs, C. T. (2002). Determining concentration and fall velocity of estuarine particle populations using ADV, OBS and LISST. *Continental Shelf Research*, *22*(11-13), 1867–1886. https://doi.org/10.1016/S0278-4343(02)00043-2

George, R., Flick, R. E., & Guza, R. T. (1994). Observations of turbulence in the surf zone. *Journal of Geophysical Research*, *99*(C1), 801–810, https://doi.org/10.1029/93JC02717

Grant, W. D., & Madsen, O. S. (1986). The continental-shelf bottom boundary layer. *Annual Review of Fluid Mechanics*, *18*(1), 265–305. https://doi.org/10.1146/annurev.fl.18.010186.001405

Grass, A. J. (1971). Structural features of turbulent flow over smooth and rough boundaries. *Journal of Fluid Mechanics*, *50*(02), 233–255. https://doi.org/10.1017/S0022112071002556

Grass, A. J. (1974). Transport of fine sand on a flat bed. Euromech 48: Transport, Erosion and Deposition of Sediment in Turbulent Streams, Technical University of Denmark, Lyngby.

Grinsted, A., Moore, J. C., & Jevrejeva, S. (2004). Application of the cross wavelet transform and wavelet coherence to geophysical time series. *Nonlinear Processes in Geophysics.*, *11*(5/6), 561–566. https://doi.org/10.5194/npg-11-561-2004

Harris, P. T., & Baker, E. K. (1988). A review of seabed sediments, morphology and acoustic properties of the outer continental shelf and upper slope, northern Australia (Gladstone to Dampier), Ocean Sciences Institute, University of Sydney Report No. 33, 56.

Heathershaw, A. D. (1979). The turbulent structure of the bottom boundary layer in a tidal current. *Geophysical Journal of the Royal Astronomical Society*, *58*(2), 395–430. https://doi.org/10.1111/j.1365-246X.1979.tb01032.x

Heathershaw, A. D., & Thorne, P. D. (1985). Seabed noises reveal role of turbulent bursting phenomenon in sediment transport by tidal currents. *Nature*, *316*(6026), 339–342. https://doi.org/10.1038/316339a0

Hino, M., Kashiwayanagi, M., Nakayama, A., & Hara, T. (1983). Experiments on the turbulence statistics and the structure of a reciprocating oscillatory flow. *Journal of Fluid Mechanics*, *131*, 363–400. https://doi.org/10.1017/S0022112083001378

Holloway, P. E. (1983). Internal tides on the Australian North-West Shelf: A preliminary investigation. *Journal of Physical Oceanography*, *13*(8), 1357–1370. https://doi.org/10.1175/1520-0485(1983)013<1357:ITOTAN>2.0.CO;2

Holloway, P. E., & Nye, H. C. (1985). Leeuwin current and wind distributions on the southern part of the Australian North West Shelf between January 1982 and July 1983. *Marine and Freshwater Research*, *36*(2), 123–137. https://doi.org/10.1071/MF9850123

Hurther, D., & Lemmin, U. (2003). Turbulent particle flux and momentum flux statistics in suspension flow. *Water Resource Research*, *39*(5), 1139. https://doi.org/10.1029/2001WR001113

Izadinia, E., Heidarpour, M., & Schleiss, A. J. (2013). Investigation of turbulence flow and sediment entrainment around a bridge pier. *Stochastic Environmental Research and Risk Assessment*, *27*(6), 1303–1314. https://doi.org/10.1007/s00477-012-0666-x

Kaftori, D., Hetsroni, G., & Banerjee, S. (1995). Particle behavior in the turbulent boundary layer. I. Motion, deposition, and entrainment. *Physics of Fluids*, *7*, 1095–1106. https://doi.org/10.1063/1.868551

Katsumata, K. (2006). Tidal stirring and mixing on the Australian North West Shelf. *Marine and Freshwater Research*, *57*(3), 243–254. https://doi.org/10.1071/MF05059

Keylock, C. J. (2007). The visualisation of turbulence data using a wavelet-based method. *Earth Surface Processes and Landforms*, *32*(4), 637–647. https://doi.org/10.1002/esp.1423

Keylock, C. J., Lane, S. N., & Richards, K. S. (2014). Quadrant/octant sequencing and the role of coherent structures in bed load sediment entrainment. *Journal of Geophysical Research: Earth Surface*, *119*, 264–286. https://doi.org/10.1002/2012JF002698

Kim, S.-C., Friedrichs, C. T., Maa, J. P.-Y., & Wright, L. D. (2000). Estimating bottom stress in tidal boundary layer from acoustic Doppler velocimeter data. *Journal of Hydraulic Engineering*, *126*(6), 399–406. https://doi.org/10.1061/(ASCE)0733-9429(2000)126:6(399)

Kline, S. J., Reynolds, W. C., Schraub, F. A., & Runstadler, P. W. (1967). The structure of turbulent boundary layers. *Journal of Fluid Mechanics*, *30*, 741–773. https://doi.org/10.1017/S0022112067001740

Kolmogorov, A. N. (1941). The local structure of turbulence in incompressible viscous fluids at very large Reynolds numbers. *Doklady Akademii Nauk SSSR*, *30*, 299–303.

Kondolf, G. M., Gao, Y., Annandale, G. W., Morris, G. L., Jiang, E., Zhang, J., et al. (2014). Sustainable sediment management in reservoirs and regulated rivers: Experiences from five continents. *Earth's Future*, *2*(5), 256–280. https://doi.org/10.1002/2013EF000184

Kularatne, S., & Pattiaratchi, C. (2008). Turbulent kinetic energy and sediment resuspension due to wave groups. *Continental Shelf Research*, *28*(6), 726–736. https://doi.org/10.1016/j.csr.2007.12.007

Kwoll, E., Venditti, J. G., Bradley, R. W., & Winter, C. (2016). Flow structure and resistance over subaquaeous high- and low-angle dunes. *Journal of Geophysical Research: Earth Surface*, *121*, 545–564. https://doi.org/10.1002/2015JF003637

Lavelle, J., & Mofjeld, H. (1987). Do critical stresses for incipient motion and erosion really exist? *Journal of Hydraulic Engineering*, *113*(3), 370–385. https://doi.org/10.1061/(ASCE)0733-9429(1987)113:3(370)

Leckie, S. H. F., Mohr, H., Draper, S., McLean, D. L., White, D. J., & Cheng, L. (2016). Sedimentation-induced burial of subsea pipelines: Observations from field data and laboratory experiments. *Coastal Engineering*, *114*, 137–158. https://doi.org/10.1016/j.coastaleng.2016.04.017

Ling, C. H. (1995). Criteria for incipient motion of spherical sediment particles. *Journal of Hydraulic Engineering*, *121*(6), 472–478. https://doi.org/10.1061/(ASCE)0733-9429(1995)121:6(472)

Liu, D., Liu, X., Fu, X., & Wang, G. (2016). Quantification of the bed load effects on turbulent open-channel flows. *Journal of Geophysical Research: Earth Surface*, *121*, 767–789. https://doi.org/10.1002/2015JF003723

Lohrmann, A. (2001). Monitoring sediment concentration with acoustic backscattering instruments, Nortek Tehcnical Note No.: 003, 1–5.

Lu, S. S., & Willmarth, W. W. (1973). Measurements of the structure of the Reynolds stress in a turbulent boundary layer. *Journal of Fluid Mechanics*, *60*(03), 481–511. https://doi.org/10.1017/S0022112073000315

Mao, Y. (2003). The effect of turbulent bursting on the sediment movement in suspension. *International Journal of Sediment Research*, *18*, 148–157.

McLelland, S. J., & Nicholas, A. P. (2000). A new method for evaluating errors in high-frequency ADV measurements. *Hydrological Processes*, *14*(2), 351–366. https://doi.org/10.1002/(SICI)1099-1085(20000215)14:2<351::AID-HYP963>3.0.CO;2-K

Mei, C. C., Fan, S.-j., & Jin, K.-r. (1997). Resuspension and transport of fine sediments by waves. *Journal of Geophysical Research*, *102*(C7), 15,807–15,821. https://doi.org/10.1029/97JC00584

Meuleners, M. J., Pattiaratchi, C. B., & Ivey, G. N. (2007). Numerical modelling of the mean flow characteristics of the Leeuwin current system. *Deep Sea Research Part II: Topical Studies in Oceanography*, *54*(8-10), 837–858. https://doi.org/10.1016/j.dsr2.2007.02.003

Nelson, J. M., Shreve, R. L., McLean, S. R., & Drake, T. G. (1995). Role of near-bed turbulence structure in bed load transport and bed form mechanics. *Water Resources Research*, *31*(8), 2071–2086. https://doi.org/10.1029/95WR00976

Nikora, V., Goring, D., & Ross, A. (2002). The structure and dynamics of the thin near-bed layer in a complex marine environment: A case study in Beatrix Bay, New Zealand. *Estuarine, Coastal and Shelf Science*, *54*(5), 915–926. https://doi.org/10.1006/ecss.2001.0865

Niño, Y., & Garcia, M. H. (1996). Experiments on particle—Turbulence interactions in the near–wall region of an open channel flow: Implications for sediment transport. *Journal of Fluid Mechanics*, *326*, 285–319. https://doi.org/10.1017/S0022112096008324

Niño, Y., Lopez, F., & Garcia, M. (2003). Threshold for particle entrainment into suspension. *Sedimentology*, *50*(2), 247–263. https://doi.org/10.1046/j.1365-3091.2003.00551.x

O'Callaghan, J. M., Pattiaratchi, C. B., & Hamilton, D. P. (2010). The role of intratidal oscillations in sediment resuspension in a diurnal, partially mixed estuary. *Journal of Geophysical Research*, *115*, C07018. https://doi.org/10.1029/2009JC005760

Pattiaratchi, C. B., & Collins, M. B. (1985). Sand transport under the combined influence of waves and tidal currents: An assessment of available formulae. *Marine Geology*, *67*, 83–100. https://doi.org/10.1016/0025-3227(85)90149-5

Pope, N. D., Widdows, J., & Brinsley, M. D. (2006). Estimation of bed shear stress using the turbulent kinetic energy approach—A comparison of annular flume and field data. *Continental Shelf Research*, *26*, 959–970. https://doi.org/10.1016/j.csr.2006.02.010

Robinson, J. E., Newell, R. C., Seiderer, L. J., & Simpson, N. M. (2005). Impacts of aggregate dredging on sediment composition and associated benthic fauna at an offshore dredge site in the southern North Sea. *Marine Environmental Research*, *60*(1), 51–68. https://doi.org/10.1016/j.marenvres.2004.09.001

Robinson, S. K. (1991). Coherent motions in the turbulent boundary layer. *Annual Review of Fluid Mechanics*, *23*(1), 601–639. https://doi.org/10.1146/annurev.fl.23.010191.003125

Salim, S., Pattiaratchi, C., Tinoco, R., Coco, G., Hetzel, Y., Wijeratne, S., & Jayaratne, R. (2017). The influence of turbulent bursting on sediment resuspension under fluvial unidirectional currents. *Earth Surface Dynamics*, 1–17. https://doi.org/10.5194/esurf-2016-60

Shalaby, H. H. (2007). On the potential of large eddy simulation to simulate cyclone separators, (PhD thesis). Chemnitz University of Technology, Chemnitz.

Shi, B. W., Wang, Y. P., Yang, Y., Ni, W. F., Li, P., & Gao, J. H. (2015). Determination of critical shear stresses for erosion and deposition based on in situ measurements of currents and waves over an intertidal mudflat. *Journal of Coastal Research*, *31*(6), 1344–1356.

Shields, A. F. (1936). Application of similarity principles and turbulence research to bed-load movement, Mitteilungen der Preussischen Versuchsanstalt f€ur Wasserbau und Schiffbau, Berlin, Germany (pp. 5-24).

Simpson, R. L. (1989). Turbulent boundary layer separation. *Annual Review of Fluid Mechanics*, *21*(1), 205–232. https://doi.org/10.1146/annurev.fl.21.010189.001225

Smyth, C., & Hay, A. E. (2003). Near-bed turbulence and bottom friction during SandyDuck97. *Journal of Geophysical Research*, *108*(C6), 3197. https://doi.org/10.1029/2001JC000952

Soulsby, R. (1997). *Dynamics of marine sands* (pp. 99–110). London, UK: Thomas Telford Publications.

Soulsby, R. L. (1983). In B. Johns (Ed.), *"The bursting phenomenon", in Physical oceanography of coastal and shelf seas*, *Elsevier Oceanography Series* (Vol. 35, p. 470). Amsterdam, The Netherlands: Elsevier Science Publishers.

Soulsby, R. L., Atkins, R., & Salkield, A. P. (1994). Observations of the turbulent structure of a suspension of sand in a tidal current. *Continental Shelf Research*, *14*(4), 429–435, https://doi.org/10.1016/0278-4343(94)90027-2

Soulsby, R. L., & Whitehouse, R. J. S. (1997). Threshold of sediment motion in coastal environments. Proceedings of the combined Australasian coastal engineering and port conference, Christchurch, 7–11 September 1997 (pp. 149–154).

Sumer, B. M., & Deigaard, R. (1981). Particle motions near the bottom in turbulent flow in an open channel. Part 2. *Journal of Fluid Mechanics*, *109*, 311–337. https://doi.org/10.1017/S0022112081001092

Sumer, B. M., & Oguz, B. (1978). Particle motions near the bottom in turbulent flow in an open channel. *Journal of Fluid Mechanics*, *86*, 109–127. https://doi.org/10.1017/S0022112078001020

Sutherland, A. J. (1967). Proposed mechanism for sediment entrainment by turbulent flows. *Journal of Geophysical Research*, *72*(24), 6183–6194. https://doi.org/10.1029/JZ072i024p06183

Taylor, G. I. (1938). The spectrum of turbulence. *Proceedings of the Royal Society of London A: Mathematical, Physical and Engineering Sciences*, *164*(919), 476–490, https://doi.org/10.1098/rspa.1938.0032.

Thompson, C. E. L., Kassem, H., & Williams, J. (2013). Nearshore sediment resuspension and bed morphology. *Journal of Coastal Research*, *165*, 1593–1598. https://doi.org/10.2112/SI65-269.1

Thorne, P. D., Williams, J. J., & Heathershaw, A. D. (1989). In situ acoustic measurements of marine gravel threshold and transport. *Sedimentology*, *36*(1), 61–74. https://doi.org/10.1111/j.1365-3091.1989.tb00820.x

Van de Kreeke, J., Day, C. M., & Mulder, H. P. J. (1997). Tidal variations in suspended sediment concentration in the Ems estuary: Origin and resulting sediment flux. *Journal of Sea Research*, *38*, 1–16.

van Rijn, L. C. (1984). Sediment transport, Part I: Bed load transport. *Journal of Hydraulic Engineering*, *110*(10), 1431–1456. https://doi.org/10.1061/(ASCE)0733-9429(1984)110:10(1431)

Velikanov, M. A. (1955). *Dynamics of alluvial stream, 2, State Publishing House of Theoretical and Technical* (in Russian). Russia: Literature.

Voulgaris, G., & Meyers, S. T. (2004). Temporal variability of hydrodynamics, sediment concentration and sediment settling velocity in a tidal creek. *Continental Shelf Research*, *24*(15), 1659–1683. https://doi.org/10.1016/j.csr.2004.05.006

Voulgaris, G., & Trowbridge, J. H. (1998). Evaluation of the acoustic Doppler velocimeter (ADV) for turbulence measurements. *Journal of Atmospheric and Oceanic Technology*, *15*(1), 272–289. https://doi.org/10.1175/1520-0426(1998)015<0272:eotadv>2.0.co;2

Wang, Y. Y., He, Q., & Liu, H. (2009). Variations of near-bed suspended sediment concentration in south passage of the Changjiang Estuary. *Journal of Sediment Research*, *12*(6), 6–13.

Westra, S., Brown, C., Lall, U., Koch, I., & Sharma, A. (2010). Interpreting variability in global SST data using independent component analysis and principal component analysis. *International Journal of Climatology*, *30*, 333–346. https://doi.org/10.1002/joc.1888

Wolanski, E., Richmond, R. H., Davis, G., & Bonito, V. (2003). Water and fine sediment dynamics in transient river plumes in a small, reef-fringed bay, Guam. *Estuarine, Coastal and Shelf Science*, *56*, 1029–1040. https://doi.org/10.1016/S0272-7714(02)00321-9

Wu, F. C., & Chou, Y. J. (2003). Rolling and lifting probabilities for sediment entrainment. *Journal of Hydraulic Engineering*, *129*(2), 110–119. https://doi.org/10.1061/(ASCE)0733-9429(2003)129:2(110)

Wu, F.-C., & Shih, W.-R. (2012). Entrainment of sediment particles by retrograde vortices: Test of hypothesis using near-particle observations. *Journal of Geophysical Research*, *117*, F03018. https://doi.org/10.1029/2011JF002242

Yang, Y., Wang, Y. P., Gao, S., Wang, X. H., Shi, B. W., Zhou, L., et al. (2016). Sediment resuspension in tidally dominated coastal environments: New insights into the threshold for initial movement. *Ocean Dynamics*, *66*(3), 401–417. https://doi.org/10.1007/s10236-016-0930-6

Yuan, Y., Wei, H., Zhao, L. A., & Cao, Y. N. (2009). Implications of intermittent turbulent bursts for sediment resuspension in a coastal bottom boundary layer: A field study in the western Yellow Sea, China. *Marine Geology*, *263*(1-4), 87–96. https://doi.org/10.1016/j.margeo.2009.03.023